J Mater Sci (2023) 58:369–382

Materials for life sciences

An oxidative polymerized carboxymethyl cellulose hydrogel for the combined anti-tumor recurrence

Yangbei Zhu[1], Yu Zhang[2], Hang Wu[3], Shige Wang[2], and Xinghua Li[1,*]

[1] *Endoscopy Center and Endoscopy Research Institute, Zhongshan Hospital, Fudan University, No. 180 Fenglin Road, Xuhui District, Shanghai 200032, People's Republic of China*

[2] *School of Materials and Chemistry, University of Shanghai for Science and Technology, No. 516 Jungong Road, Shanghai 200093, People's Republic of China*

[3] *Department of Gastroenterology, Changhai Hospital, Naval Medical University, No. 168 Changhai Road, Shanghai 200433, People's Republic of China*

Received: 2 July 2022
Accepted: 30 November 2022
Published online: 1 January 2023

ABSTRACT

Malignant tumor has always been a complex disease that endangers human health. Traditional treatment methods include surgical resection, chemotherapy, and radiotherapy. However, solid tumors are prone to recur. Herein, we developed a hydrogel-based drug-carrying system to prevent postoperative tumor recurrence. Sodium carboxymethyl cellulose was modified with dopamine via the *N*-hydroxysuccinimide (NHS) and 1-ethyl-(3-dimethylaminopropyl) carbanyl diimide (EDC)-mediated coupling chemistry. The CMC-DA-MnO_2/MnO (CDM) hydrogel was prepared by oxidative cross-linking, using $KMnO_4$ as the oxidizing agent. In the hydrogel, the $KMnO_4$ can not only be used as an oxidant to trigger the polymerization and gelation of CMC-DA but also transformed into MnO_2 and MnO to afford the T_2-weighted magnetic resonance imaging (MRI). The fluorescent dye IR808 as a photosensitizer was introduced into the hydrogel system by simply soaking the CDM hydrogel in the IR808 solution. Under the 808 nm laser irradiation, IR808 and PDA endowed the hydrogel with tumor photodynamic therapy (PDT) and photothermal therapy (PTT) capacities, respectively. With the proven hemo- and cyto-compatibilities, the CDM hydrogel was successfully used for the PDT and PTT prevention of postoperative tumor recurrence.

Handling Editor: Yaroslava Yingling.

Yangbei Zhu and Yu Zhang have contributed equally to this work.

Address correspondence to E-mail: lixinghua2002@aliyun.com

https://doi.org/10.1007/s10853-022-08046-2

Introduction

The present main clinical cancer therapies include surgery, radiotherapy, and chemotherapy, which have certain therapeutic effects on most tumors [1, 2]. However, solid tumors are prone to recurrence and metastasis. Photothermal therapy (PTT), as a new cancer treatment approach, employs a photothermal conversion agent and light to produce heat and kill cancer cells [3, 4]. Compared with other tumor treatment methods, PTT shows several advantages like easy operation, and minimal or non-invasive to normal tissues [5–7]. Moreover, most kinds of photothermal materials are easily functionalized with other molecules such as drug molecules and photosensitizers for combined tumor therapy. Photodynamic therapy (PDT) is an alternative method that has been successfully used to treat many malignant tumors [8–10]. During tumor PDT, the energy of the laser was absorbed by the photosensitizer which can convert the oxygen into cytotoxic reactive oxygen species (ROS) for cancer cell killing [11–13]. A prominent advantage of PDT is that it has an admirable spatiotemporal selectivity. Therefore, PDT holds the potential to reduce damage to normal tissues [14, 15]. However, due to the short service life of ROS, the therapeutic efficiency of PDT is always limited [16]. In addition, photosensitizer, as a small molecule drug, is difficult to effectively accumulate in tumor sites and its non-specific biodistribution may bring undesired side effects to normal tissues [17, 18].

Despite the continuous improvement of tumor PTT and PDT, they can still cause recurrence since a few cancer cells, which is enough to cause a fatal recurrence. An alternative method to overcome these shortcomings is to use hydrogel as a drug carrier, which provides a high-dose accumulation and sustained drug release in the pathological site [19]. Hydrogels are usually composed of hydrophilic polymers and have a three-dimensional cross-linked network that can retain a large amount of water [20]. Most kinds of hydrogel are biocompatible and have become valuable candidates in the field of biomedicine [21]. Besides, hydrogels can control the release of the drug since they have a network structure. With unique advantages like robust biodegradability, biocompatibility, and low cost, natural polymers have shown bright application prospects in the preparation of hydrogels. Cellulose is the main component of lignocellulosic biomass and one of the most abundant natural polymers in nature [22]. Cellulose and its derivatives are biocompatible, biodegradable, and renewable, and it has abundant active groups that can afford various functionalizations [23]. Therefore, they have attracted ever-increasing attention in the field of biomedicine [24, 25]. Dopamine (DA) is a biocompatible neurotransmitter in the human body [26], which can self-polymerize into polydopamine (PDA) with photothermal properties and has been frequently applied in tumor PTT and other fields [27–29]. However, the combination of cellulose with polydopamine for tumor therapy application has been rarely studied.

Herein, we developed an implantable CMC-DA-MnO_2/MnO (CDM) hydrogel with tumor PTT and PDT capacities to prevent postoperative tumor recurrence (Scheme 1). Specifically, sodium carboxymethyl cellulose (CMC-Na) was activated by *N*-hydroxysuccinimide (NHS) and 1-ethyl-(3-dimethylaminopropyl) carbanyl diimide (EDC), and then, DA was introduced to obtain a dopamine-modified CMC-Na. Potassium permanganate ($KMnO_4$) was further used to oxidize the dopamine-modified CMC-Na. This process successfully endowed the hydrogel with light-to-heat conversion property since DA was oxidized into PDA by $KMnO_4$. Then, the photosensitizer IR808 was physically absorbed by the CDM hydrogel to simultaneously realize the tumor PDT. Both in vivo and in vitro experiments verified that CDM/IR808 hydrogel has a good anti-tumor effect and was used to effectively prevent postoperative tumor recurrence in this study.

Experiment section

Synthesis of CMC-DA and hydrogels

A 1.25 g CMC-Na was dissolved in 100 mL citrate buffer solution (CBS, pH = 5.4) at 35 °C. Then, 2.3942 g EDC and 1.1978 g NHS were added to activate the CMC-Na for 20 min. The solution was added with DA·HCl (2.0 g) and stirred for 24 h [30]. Finally, the product was dialyzed with deionized water for 3 days using a dialysis bag with a cut-off molecular weight of 14,000 Da. Dopamine-modified sodium carboxymethyl cellulose (CMC-DA) was freeze-dried and stored in a refrigerator at 4 °C. The CDM hydrogel was prepared by mixing 1 mL of CMC-DA

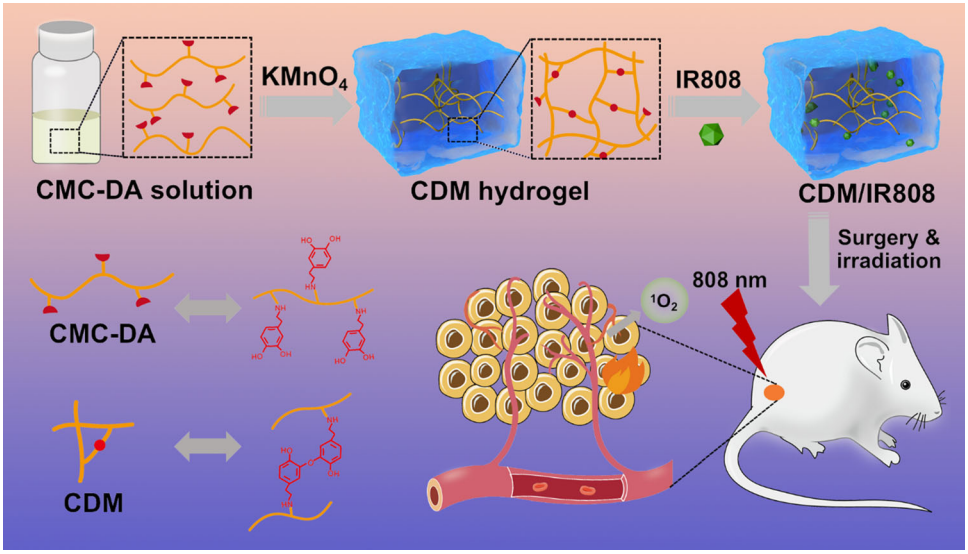

Scheme 1 The illustration of CMC-DA preparation, $KMnO_4$-induced hydrogel formation, IR808 loading, and the combined anti-tumor recurrence.

solution (30 mg/mL in 0.1 M phosphate-buffered saline (PBS)) with 0.25 mL of $KMnO_4$ solution (50 mM, in water). Time–viscosity relationship was monitored using Brookfield Viscometer, RV-T (rotation speed: 10 rpm) within the first 30 s according to the instruction. The determination of the porosity of the hydrogel is as follows: immersing the pre-weighed freeze-dried hydrogel into 30 min of 4 mL absolute ethanol, and then removing the hydrogel and weighing again. The porosity is calculated as follows:

$$Porosity\% = \frac{N_1 - N_0}{\rho V_0} \times 100\%$$

In this equation, N_0 and N_1, respectively, indicate the weight of hydrogel before and after immersion in absolute ethanol. V_0 is the volume of hydrogel samples, and ρ is the density of absolute ethanol (0.785 g/cm^3).

In vitro degradation of the hydrogel

The weight change of CDM hydrogel in CBS that mimics the weakly acidic tumor microenvironment was studied to assess the degradation performance. For this purpose, the lyophilized hydrogel was immersed in CBS at 37 °C for 1, 2, 3, 5, 7, 14, 21, or 28 days. Then, the hydrogel was taken out and rinsed with deionized water three times. After being freeze-dried, the hydrogels were weighed. The residual gel weight was calculated according to the following formula: Gel weight = $\frac{W_t}{W_0} \times 100\%$ (W_t and W_0 are the real-time quality and the initial quality of CDM hydrogel, respectively). In addition, the images of hydrogels after 0, 7, 14, 28, or 56 days of incubation were recorded.

IR808 loading

To prepare the IR808 solution, it was dissolved in absolute ethanol and then diluted using deionized water. In terms of photosensitizer loading, 0.1 g of dry CDM hydrogel was continuously soaked in 50, 100, or 200 μg/mL IR808 solutions for 12 h at room temperature. After that, the hydrogel was taken out and washed with distilled water, the left solution was collected and its absorbance at 787 nm was read using the ultraviolet–visible-near-infrared (UV–Vis-NIR) spectrometer (Lambda 25, PerkinElmer, USA) to quantify the concentration of unloaded IR808 according to the absorbance-concentration calibration curve. The IR808 loading efficiency was calculated by dividing the loaded IR808 mass by the total IR808 mass. The IR808 loading percentage was calculated by dividing the mass of the loaded IR808 by the mass of CDM/IR808 hydrogel. The IR808-loaded hydrogel was stored in a refrigerator at 4 °C in the dark.

Detection of ROS

A commonly used ROS indicator, diphenylisobenzofuran (DPBF) was used to detect the ROS production of CDM/IR808 hydrogel. The generation of ROS was detected by observing the change in the absorption peak intensity of the DPBF solution.

Specifically, 0.1 g of CDM/IR808 hydrogel was immersed in DPBF solution (3 mL, 33.33 μg/mL). Under dark, an 808 nm laser (0.15 W/cm^2) was used to irradiate the hydrogel. The light absorption of the supernatant after 0, 2, 4, 6, 8, or 10 min of irradiation was recorded using the Uv–Vis-NIR spectrophotometer (Lambda 25, PerkinElmer, USA). The pure DPBF solution that irradiated with the 808 nm laser (0.15 W/cm^2) for 10 min as a control.

Photothermal conversion of hydrogels

The 808 nm NIR laser with the power density of 1.0 W/cm^2, 0.8 W/cm^2, or 0.5 W/cm^2 was used to irradiate the hydrogel (10 mg, soaked in 100 μL of saline) in a 96-well cell plate. The real-time temperature was recorded with the infrared thermal imaging system (FLIR E60, USA). To study the photothermal stability, the hydrogel was irradiated (0.8 W/cm^2, 5 min) and then cooled to room temperature (laser turned off for 5 min), and the process was repeated 6 times. The light-to-heat conversion efficiency (η) was calculated based on the cooling curve of the hydrogel, using the following formula [31, 32], $\eta = \frac{hS(T_{max}-T_{surr})-Q_{dis}}{I\left(1-10^{-A_\lambda}\right)}$. More details for the calculation of η were listed in the supporting information.

In vitro hemocompatibility

A 2 mL of whole blood from healthy Kunming (KM) mice was centrifuged for 3 min (3000 rpm) to obtain erythrocytes. After washing 3 times with PBS, a suspension of erythrocytes in PBS was prepared at a volume ratio of 1:25 and stored at 4 °C. For the experiment, 1.0 mL of the above erythrocyte was mixed with 3.0 mL of deionized water (positive control), 3.0 mL of PBS (negative control), or CDM hydrogel (10 mg/mL or 20 mg/mL) as the experimental group. The erythrocytes were placed in a 37 °C incubator and cultured for 2 h. Then, the hydrogel was discarded and centrifuged (3000 rpm, 5 min) to obtain the supernatant. The absorbance at 541 nm of the supernatant which is the characteristic absorption wavelength of hemoglobin was measured. The hemolysis ratio was calculated: $\text{Hemolysis ratio}(\%) = \frac{(D_t-D_{nc})}{(D_{pc}-D_{nc})} \times 100\%$. In this equation, D_{pc}, D_{nc}, and D_t refer to the absorbance values of the supernatant solution of erythrocytes treated with PBS, deionized water, and hydrogel, respectively.

In vitro biocompatibility

In this study, the hydrogel extract was prepared by immersing the sterilized hydrogel in a serum-free cell culture medium and continuously cultured for 24 h (37 °C), with a concentration of 100 mg extract in 1 mL medium. Subsequently, the extract was sterilized with a filter membrane (0.22 μm) and diluted with culture medium to 100 mg/mL, 50 mg/mL, 20 mg/mL, and 10 mg/mL. Then, mouse fibroblast (L929) cells were selected to evaluate the biological effect of hydrogels. These cells were cultured with the hydrogel extract for 24 h or 48 h. After that, cell counting kit-8 (CCK-8) analysis was performed to test the cell viability. We used a microplate reader to measure the absorbance of all samples at 450 nm. The staining of live and dead cells was also collected using a Dead/Live staining kit with an inverted phase-contrast microscope (Leica DM IL, Germany).

In vivo biocompatibility

All animal experimental procedures were approved by the Institutional Animal Care and Use Committee of the First Affiliated Hospital of Naval Medical University (Changhai Hospital). In our research, we used weight monitoring, serum biochemical analyzing (using Beckman-Coulter-Unicel-doc800 automatic biochemical analyzer), blood routine test (using Sysmex-XS-800i automatic blood analyzer), tissues pathology, and element (Mn) metabolism to verify the in vivo biosafety of CDM hydrogel. For the above purposes, 50 mg of CDM hydrogel was implanted under the skin of KM mice, and mouse blood was collected on the 7th and 28th days after that. Healthy mice that received no treatment served as a control group. In addition, skin tissue sections of major organs and subcutaneous embedding sites were taken on the 0 (control), 7th, and 28th days for hematoxylin–eosin (H&E) staining. During this period, the body weight was monitored to estimate the potential adverse reactions in all groups.

In vitro cancer cells killing effect

The cultured human colorectal carcinoma (HT29) cells were seeded in a 96-well culture plate for 24 h

before 25 mg of CDM or CDM/IR808 were added to each well. The cells in the experimental group (CDM or CDM/IR808 group) were irradiated with the NIR laser (808 nm, 0.8 W/cm^2, 5 min), and the control group did not receive any treatment. After the irradiation, the hydrogel was taken out and the cells were stained and the cell morphology was observed under a microscope (Leica DM IL, Germany). The viability of the irradiated HT29 cells was measured using the CCK-8 method.

In vivo anti-recurrence of tumor

To form a typical tumor model, 100 μL of serum-free DMEM containing 1×10^7 HT29 cells was injected into the back of a Balb/c mouse. After being fed for about 2 weeks, a tumor with a diameter of approximately 0.5 cm was observed on its back. Tumor-bearing mice were randomly divided into 3 groups ($n = 4$): control, CDM hydrogel, and CDM/IR808 hydrogel groups. An incision was made at the edge of the tumor to surgically remove the tumor tissue. Then, the CDM hydrogel (0.1 g) or CDM/IR808 hydrogel (0.1 g) was implanted at the surgical site. As a control group, mice treated with saline (0.1 mL) were used to compare their anti-recurrence effects. All mice received 808 nm laser irradiation (0.8 W/cm^2, 5 min), and the thermograph and temperature of each mouse during the laser radiation were recorded (FLIR E60, USA). The tumor volume of mice in each group was measured and calculated every few days. For the in vivo T_2-weighted magnetic resonance imaging (MRI), mice in control and CDM hydrogel groups were anesthetized and scanned by a 3.0 T clinical MRI instrument. Histological examinations included hematoxylin and eosin (H&E) staining, terminal-deoxynucleotidyl transferase-mediated nick end labeling (TUNEL), and an immunohistochemical assay of Ki67 were carried out on day 14 for the assessment of therapy efficacy. For these assays, different tumors were fixed with 10% formalin at 4 °C and then embedded in paraffin to cut into slices (thickness: 8 μm). After the stain, these slices were observed using a Leica DM IL LED inverted phase-contrast microscope.

Statistical analysis

The one-way ANOVA was used to calculate the significant differences. The p-value of 0.05 was chosen as the significance level, and (*) for $p < 0.05$, (**) for $p < 0.01$, and (***) for $p < 0.001$.

Results and discussions

Hydrogel preparation and characterization

In this study, CMC-DA was synthesized via the EDC/NHS coupling chemistry, during which the carboxyl group of the CMC-Na backbone and the amino group of DA undergo an amidation reaction. Therefore, after oxidation, the distribution of PDA is more uniform than the stepwise addition of PDA. The CDM hydrogel showed photothermal conversion properties without the need for other photothermal agents. Instead, the photothermal performance and MRI imaging capability were realized simultaneously with the gelatinization process. Moreover, the singlet oxygen production and photothermal conversion were synchronously achieved when irradiated with a single 808 nm laser. Figures 1a, b shows that the CMC-DA solution underwent a sol–gel transition upon contacting the $KMnO_4$ solution, which can be ascribed to the oxidation of catechol to quinone groups by $KMnO_4$ [33, 34]. The SEM observation confirms that the prepared CDM hydrogel has a porous structure (Fig. 1c, d), which will facilitate efficient drug loading and sustained drug release. The porosity of CDM hydrogel was calculated as 24.90% ± 3.62%. Such porosity is important for the biomedical applications of hydrogels, as it can facilitate the transport of cellular nutrients. Furthermore, the elemental mapping suggests that the MnO_2 and MnO were uniformly doped in the matrix of the hydrogel (Fig. 1e-j). Figure 2a shows that CMC-DA has an obvious light absorption at 290 nm and represents the successful grafting of DA onto the CMC-Na. In the FTIR spectra (Fig. 2b), the CMC spectrum has an O–H peak at 3421 cm^{-1}, a C–H peak at 2917 cm^{-1}, and an asymmetric C=O vibration peak at 1616 cm^{-1}. The new absorption peak that appears at 1060 cm^{-1} in the CMC-DA spectrum is the peak of the generated C–N amide bond. The ^{1}H NMR spectra were further collected (figure S1). A new signal at approximately 6.8 ppm in CMC-DA corresponds to the protons of the catechol group was detected. The above results confirm that an amide bond is formed between the carboxyl group of CMC-Na and the amine group of DA. The hydrogel formation is

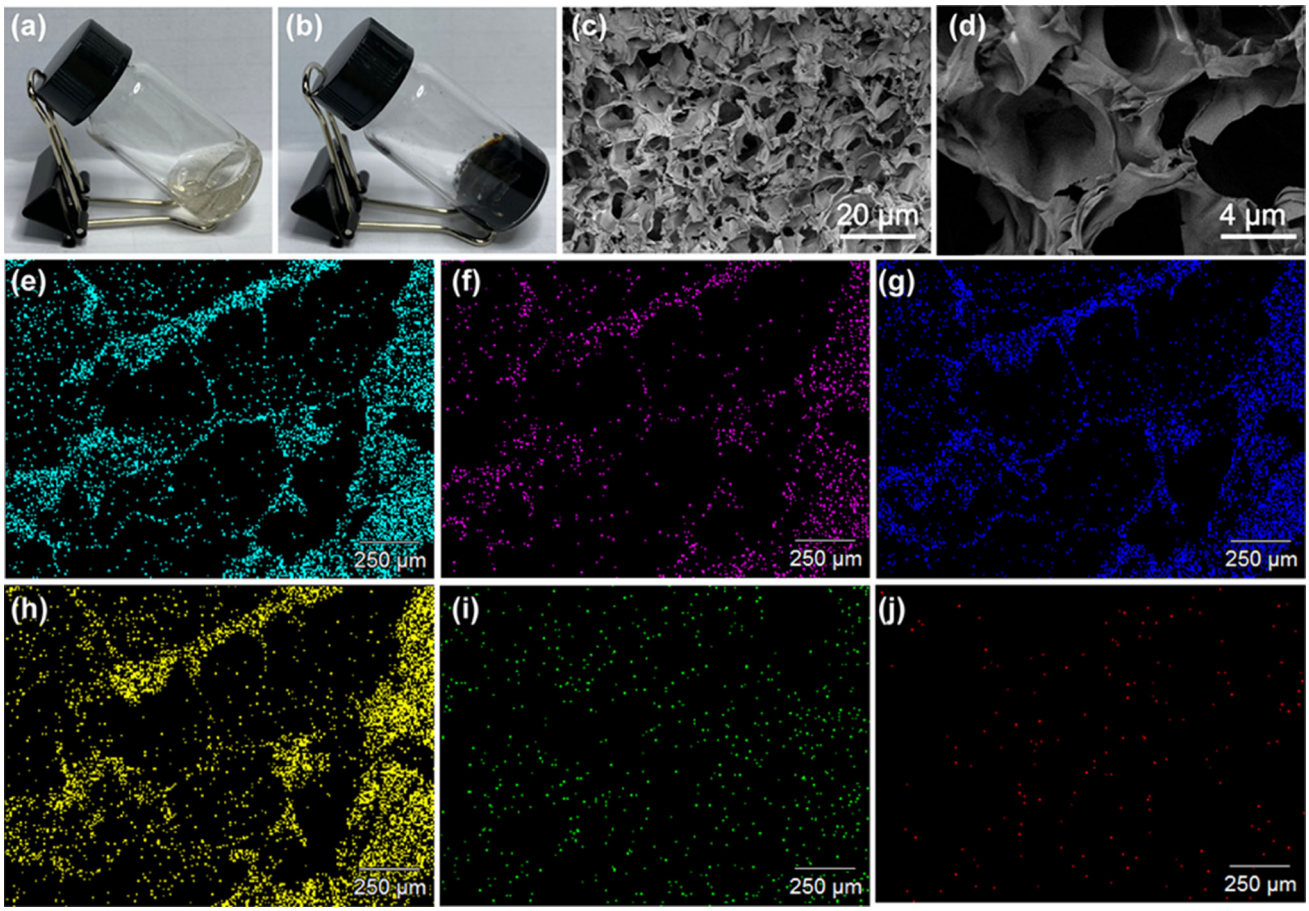

Figure 1 Digital photographs of **a** CMC-DA solution and **b** CDM hydrogel; **c**, **d** FESEM images show the morphology of CDM hydrogel; **e**–**j** C, N, O, Na, K, and Mn element distribution mappings of CDM hydrogel.

because of the polymerization of CMC-DA in the presence of $KMnO_4$, during which the CMC chains were cross-linked with each other. After the hydrogel formation, $KMnO_4$ was transformed into MnO_2 and MnO (Fig. 2c). The peaks at 652.5 eV (2p 1/2) and 642.2 eV (2p 3/2) could be, respectively, attributed to MnO_2, and the peaks at 653.8 eV (2p 1/2) and 640.8 eV (2p 3/2) could be attributed to MnO. Based on the XPS fitting results, the molar ratio of MnO_2 and MnO was about 0.9:1. Moreover, the viscosity of CDM/$KMnO_4$ solution increased gradually (figure S2), indicating that CMC-DA was oxidized by $KMnO_4$ and formed hydrogels.

A three-dimensional structure is the typical feature of a hydrogel and such a unique structural feature affords the strong water-absorbing capacity of the hydrogel. Therefore, the swelling performance of hydrogels was systematically studied by calculating the weight change at 37 °C and pH of 5.4 (CBS) or 7.4 (PBS). As shown in figure S3, the equilibrated swelling rates in H_2O, PBS, and CBS are 10,233.09%, 6035.41%, and 5017.64%, respectively, showing that CDM hydrogel has high water absorption capacity. The degradation of hydrogel is an important factor that influences its biological performance. The biodegradation behavior of CDM hydrogel in CBS solution is listed in Fig. 2d. The CDM hydrogel showed a more obvious weight loss in the first week, and the total weight loss within 28 days can reach approximately 40%, suggesting that the CDM hydrogel has good biodegradability. More interestingly, the CDM hydrogel was completely dissolved by the CBS after 56 days (figure S4), indicating that the hydrogel is biodegradable. The biodegradation of CDM hydrogel may be derived from the break of molecular chains upon its contact with the body fluid, however, further research about the detailed mechanisms is needed.

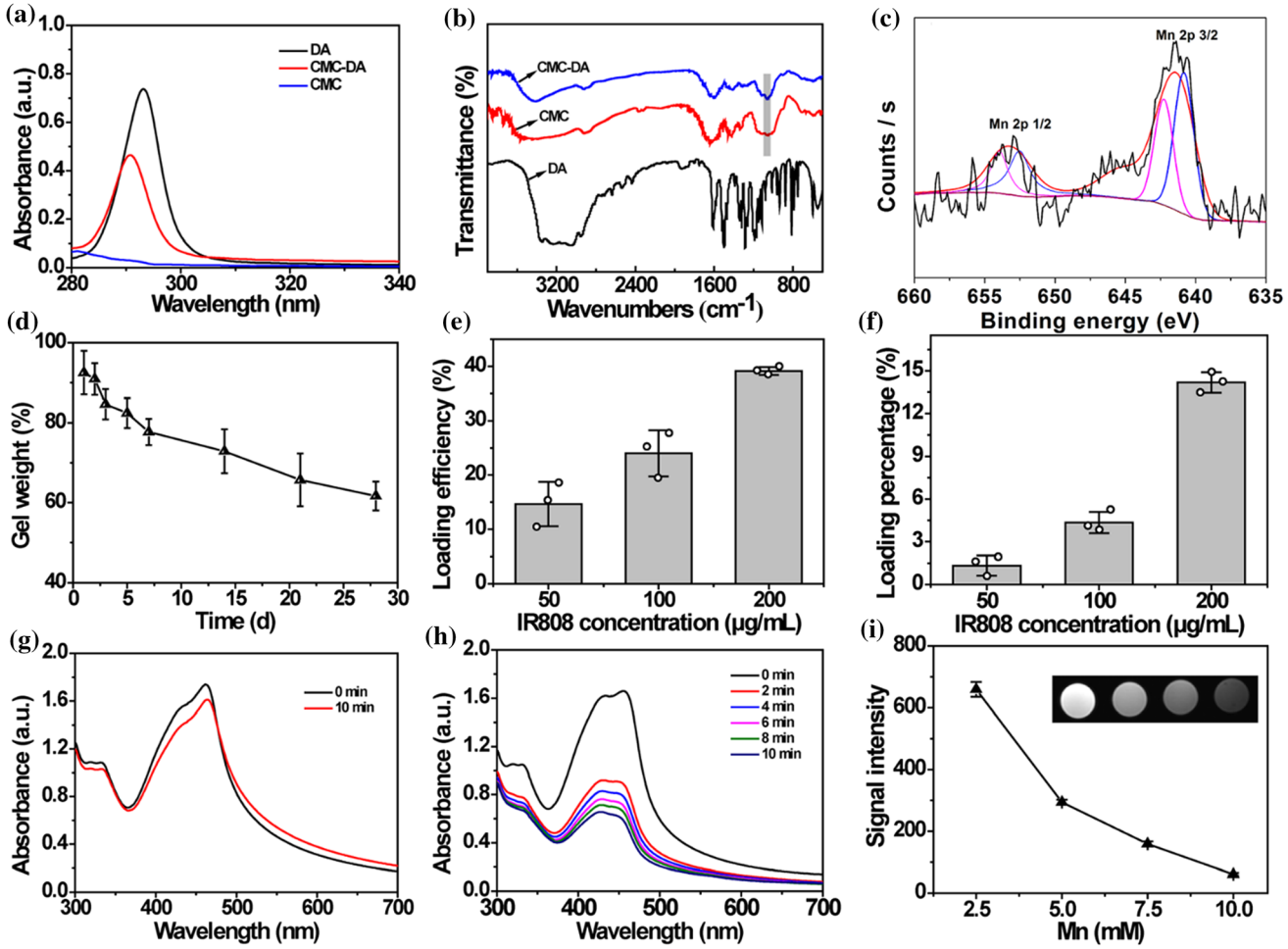

Figure 2 **a** UV–Vis spectra of DA, CMC, and CMC-DA solutions; **b** FTIR spectra of CMC, DA, and CMC-DA hydrogel; **c** XPS spectrum of Mn 2p; **d** in vitro biodegradation of CDM hydrogel in deionized water; **e** the IR808 loading efficiency of CDM hydrogel; **f** the IR808 loading percentage of CDM hydrogel; **g** the absorption spectra of pure DPBF before (0 min) and after irradiation with 808 nm laser for 10 min; **h** the absorption spectra of DPBF in the presence of CDM/IR808 hydrogel after irradiated with 808 nm laser for 0, 2, 4, 6, 8 and 10 min; **i** in vitro T_2-weighted MRI results of CDM hydrogel with different Mn concentrations (the illustration is the corresponding picture. Mn concentration: 2.5 mM, 5.0 mM, 7.5 mM, and 10.0 mM, from left to right).

In vitro IR808 loading and ROS detection

Except for the water retention, the three-dimensional structure of hydrogels also affords the loading of guest molecules. In this study, the photosensitizer IR808 was selected and absorbed by the hydrogel through physical absorption by directly dipping the hydrogel in the IR808 solution. The loading performance of CDM hydrogel was analyzed. When the concentrations of IR808 were 50, 100 and 200 μg/mL, the loading percentages of IR808 were 1.33%, 4.35%, and 14.17% (Fig. 2e), and the loading efficiencies of IR808 were calculated as 14.65%, 24.02%, and 39.12% (Fig. 2f), respectively, which is higher than the reported dye-Anchored MnO nanoparticles [4]. Based on these findings, IR808 with a concentration of 200 μg/mL was selected for the following studies. The photosensitizer loading is attributed to the diffusion of IR808 and the hydrogel matrix will act as the reservoir for the storage of these photosensitizers.

The ability of CDM/IR808 hydrogel to generate ROS under 808 nm laser irradiation was discussed, and DPBF was used as a molecular probe. The absorbance of the pure DPBF solution did not change significantly after the 10-min irradiation (Fig. 2g). However, with the prolongation of irradiation time, the absorption peak of the fluorescent probe was gradually quenched when incubated with CDM/

IR808 hydrogel (Fig. 2h), indicating that a large amount of ROS was produced. In summary, the CDM hydrogel can load the photosensitizer IR808, and the as-designed CDM/IR808 hydrogel can effectively produce ROS under laser irradiation, thereby affording the PDT of the tumor. Notably, the absorbance dropped rapidly during the first 2 min of laser exposure and was less pronounced thereafter (Fig. 2h). This is because the photosensitization was rapid and most of the DPBF was oxidized in the initial stage. In addition, CDM/IR808 was prepared by immersing the hydrogel in a photosensitizer solution, during which part of the photosensitizer was adsorbed on the hydrogel surface.

In vitro and in vivo T_2-weighted MRI

The $KMnO_4$ can not only be used as an oxidant to trigger the polymerization and gelation of CMC-DA but also transformed into MnO_2 and MnO to afford the T_2-weighted MRI. The in vitro MRI ability of CDM with different $KMnO_4$ concentrations was studied in a simulated tumor microenvironment (CBS, pH = 5.4). As shown in Fig. 2i, it is obvious that the T_2 relaxation time of water protons was shortened by the CDM hydrogel and resulting in an enhanced imaging contrast and sensitivity. Such an excellent imaging capability is anticipated to monitor the uniform distribution of the hydrogel in the tumor site. As shown in figure S5, after implanting the CDM hydrogel, the signal intensity was enhanced compared with the control group, which further proved the MRI imaging function of the CDM hydrogel. It is worth mentioning that the MnO_2 and MnO were simultaneously introduced alongside the hydrogel formation, showing its superiority to the stepwise addition. These results indicate that the CMD hydrogel holds the potential as a contrast agent for T_2-weighted MRI applications.

Photothermal conversion of hydrogel

The polymerization of dopamine causes the in situ PDA formation within the hydrogel matrix, which gives the CDM hydrogel good photothermal properties. The photothermal performances of the CDM hydrogel were evaluated by irradiating it with the 808 nm NIR laser. As shown in Fig. 3a, the temperatures of CDM hydrogel increased by 34.37 °C, 29.01 °C, and 18.61 °C, respectively, when the laser power densities are 1.0 W/cm^2, 0.8 W/cm^2, and 0.5 W/cm^2, indicating that the photothermal conversion can be adjusted by changing the power density. The corresponding thermal images are shown in Fig. 3b, which further confirms the favorable photothermal conversion of CDM hydrogel. Moreover, as shown in Fig. 3c, the temperature-rising trend of CDM hydrogel in 6 cycles did not change significantly, which proves it has favorable light-to-heat conversion durability. Finally, the η was calculated according to the cooling process as 29.74% (Fig. 3d, e). The photothermal conversion efficiency of CDM hydrogel is higher than that of polyethylene glycol-coated (PEGylated) copper nanowires [35], MoS_2-PEG nanospheres [36], and mesoporous Prussian blue@calcium phosphate [37]. Since IR808 also has a certain photothermal performance, the photothermal conversion performance of the CDM/IR808 hydrogel was also evaluated. When the power densities are 1.0 W/cm^2, 0.8 W/cm^2, and 0.5 W/cm^2, the rising temperatures of the hydrogel can reach 41.2 °C, 31.7 °C, and 17.6 °C, respectively (figure S6a), which is higher than CDM hydrogel. The corresponding thermal images are shown in figure S6b, which further confirm the good photothermal conversion performance of CDM hydrogel. After the 6 laser on/off cycles (1.0 W/cm^2), the CDM/IR808 hydrogel still exhibited a stable photothermal conversion performance (figure S6c). These data indicated that the loading of IR808 did not significantly affect the photothermal conversion of the hydrogel.

In vitro hemocompatibility

Good blood compatibility is a prerequisite for the biomedical application of hydrogel since it has the chance to directly contact the red blood cells. Therefore, the hemocompatibility of the hydrogel was studied by dispersing it in the erythrocytes/PBS dispersion with a concentration of 20 mg/mL or 10 mg/mL. As shown in figure S7a, the HP calculation showed that the hemolysis rate of the experimental group is less than 5%. The supernatant in the positive control group shows a bright red color (suggests the obvious hemolysis, figure S7b), and the supernatant of the hydrogel group is as clear as the

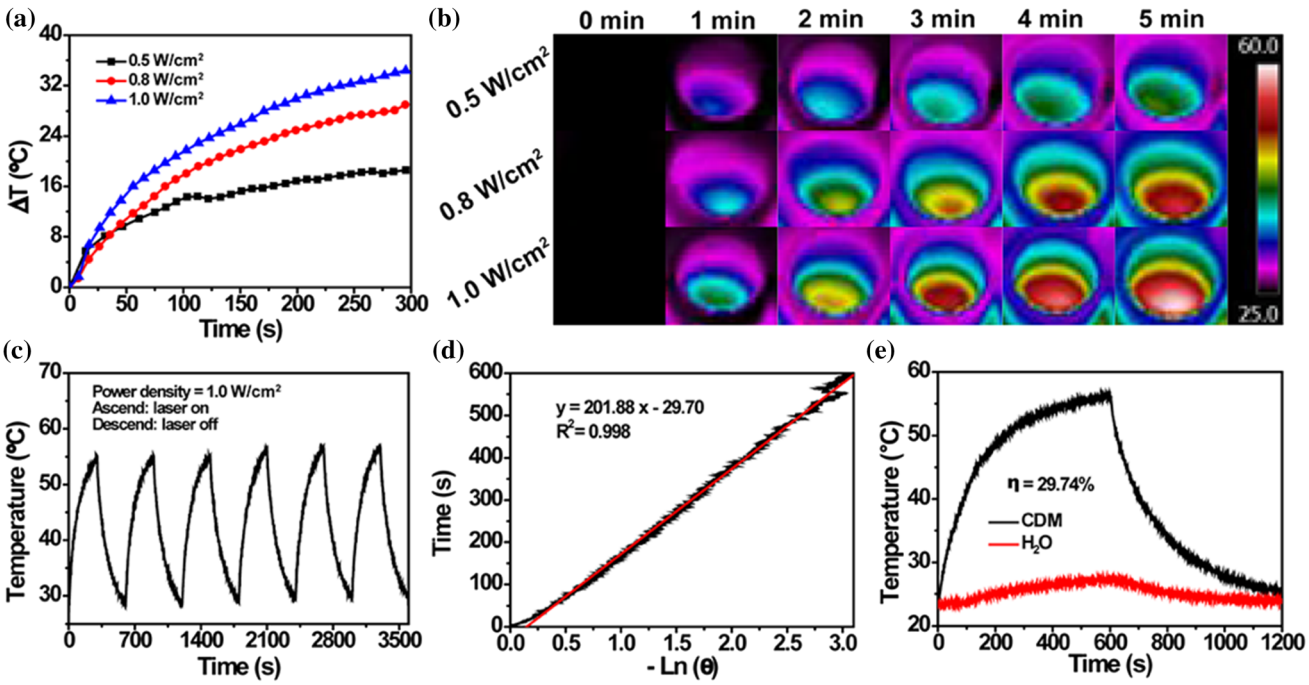

Figure 3 **a** Power density-dependent temperature increase of CDM hydrogel-containing saline under 5 min laser irradiation (808 nm; 0.5, 0.8, and 1.0 W/cm^2); **b** thermal images of CDM hydrogel corresponding to **a**; **c** the photothermal stability of CDM hydrogel in saline during 6 laser on/off cycles; **d** the time constant curve of CDM hydrogel (808 nm, 1.0 W/cm^2); **e** the η value of CDM hydrogel.

PBS group (indicates no hemolysis phenomenon, figure S7b), indicating that the CDM hydrogel has excellent blood compatibility.

In vitro biocompatibility

CMC-Na and DA are proven to be non-toxic and biodegradable [38]; therefore, the CDM hydrogel possesses favorable biocompatibility that is able to meet the requirements of biomedical applications. As shown in figure S7c, the CCK-8 assay results uncovered that after culturing cells with hydrogel extract for 24 h and 48 h, there are no significant survival rate differences between the experimental and control groups, confirming that the viability of L929 is not affected by hydrogel culture. Compared with the control group (cells cultured with normal medium), the morphology of cells in the experimental group is normal (figure S7d), revealing that the CDM hydrogel has no obvious toxicity to L929 at the experimental dose. The above results indicate that CDM hydrogel has good cell compatibility, paving the way for its secure application in the field of biomedicine.

In vivo biocompatibility

To evaluate the biological safety of CDM hydrogel in vivo, the CDM hydrogel was implanted under the skin and the animals were fed in normal conditions. Figure 4a shows that the mice's body weight changed normally within 28 days and there is no detectable difference in the mice's body weight between the experimental and control groups. The blood of the mice was collected on the 7th day and the 28th day for the in vivo hemocompatibility analysis, which proved that there was no significant difference in blood routine and various biochemical indicators in each group (Fig. 4b and S8). In addition, the H&E staining of five major organs indicated that CDM hydrogels are safe in vivo (figure S9). Stained sections of skin tissues of the CDM hydrogel implanting site also showed no inflammation (Fig. 4d-f). The in vivo biosafety of the CDM hydrogel was finalized by monitoring the content of Mn ions in the five internal organs. As shown in Fig. 4c, the Mn ions accumulation in all major organs was pretty low and gradually metabolized over time;

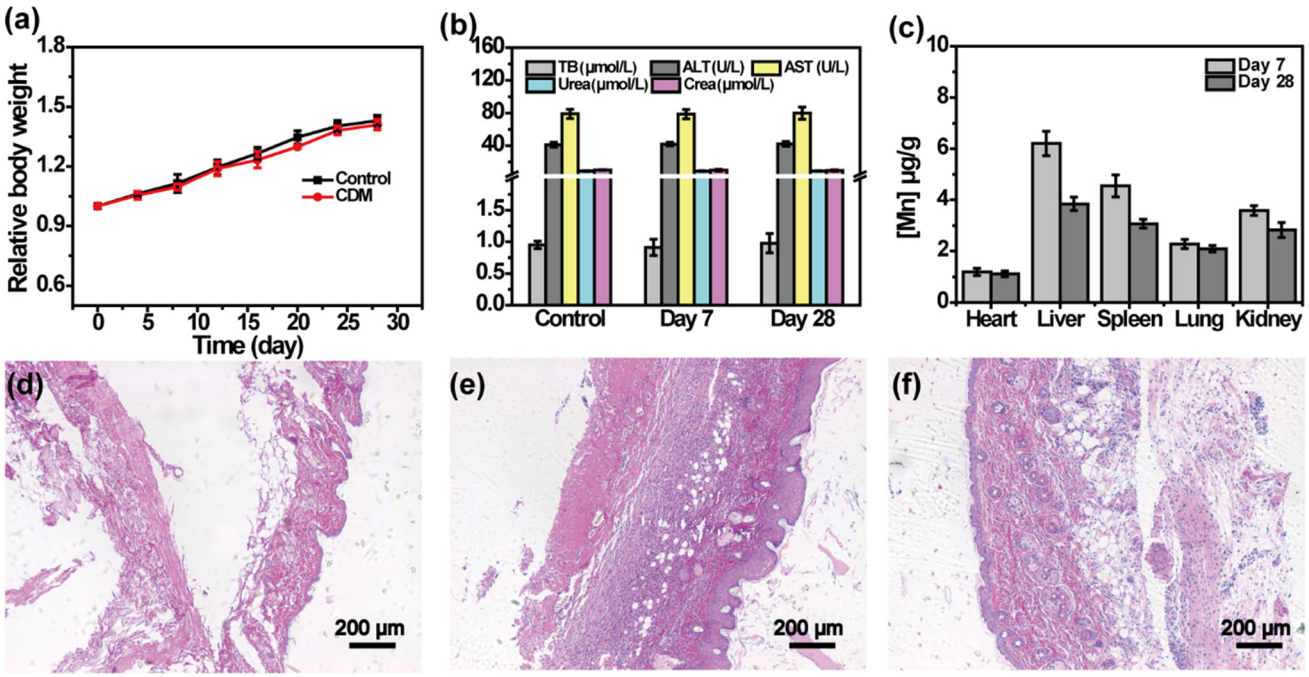

Figure 4 In vivo biocompatibility study results. **a** Relative body weight; **b** blood biochemistry parameters (total bilirubin (TB), alanine aminotransferase (ALT), aspartate aminotransferase (AST)); **c** biodistribution of Mn ions; **d-f** H&E staining results of mice skin sections treated with CDM hydrogel for (d) 0 (control), (e) 7 and (f) 28 days. Control: healthy mice that received no treatment.

therefore, the potential health risk of Mn ions can be eliminated and the in vivo biosafety is guaranteed.

In vitro cancer cells killing effect

The synergistic effect of tumor PDT and PTT at the cellular level was assessed by adding the CDM/IR808 hydrogel to the cell culture plate and irradiating it with the 808 nm laser (Fig. 5a). It was found that the cells in the control group grew well; however, when the laser was introduced in the experimental group, the survival rate of the cells in the single photothermal treatment group was 48.72% ± 1.16%, indicating that the CDM hydrogel can effectively kill cancer cells via hyperthermia. However, the cell survival rate of the synergy treatment group was as low as 10% (6.37% ± 0.80%), clearly indicating the CDM/IR808 hydrogel can synergistically kill the tumor cells under a single 808 nm irradiation. Further fluorescence staining of Dead/Live cells directly proved that CDM/IR808 can kill cancer cells more effectively than CDM (Fig. 5b–d). These results reveal the good synergistic PDT/PTT effect of CDM/IR808 hydrogel.

In vivo anti-recurrence of tumor

The in vivo synergistic PDT/PTT effect of CDM/IR808 hydrogel was confirmed in the prevention of postoperative tumor recurrence. After removing the tumor nodule, the tumor resection site was implanted with CDM or CDM/IR808 hydrogel. The control group did not implant any hydrogel. The temperature change of the tumor area was recorded (Fig. 6a, b). The thermal image showed that a rapid temperature increase of 26.62 °C of the tumor site was found after 5 min of irradiation. Under the same laser power density, the temperature change in the control group was 11.72 °C, which is significantly lower than the experimental group. The tumor growth curve and photographs showed that CDM can slightly inhibit tumor recurrence (Fig. 6c, d). Even though different kinds of theranostics or photosensitizers can kill all tumor cells, they usually used a high laser power (higher than 1 W/cm^2, for example, 3.5 W/cm^2) or alternating laser irradiation [39, 40]. As shown in Fig. 6, PTT cannot completely kill tumor cells, this is because we used a lower power density. The size of the recurring tumor in the single treatment group grows to 109.42 ± 41.63 mm^3. However, the tumor

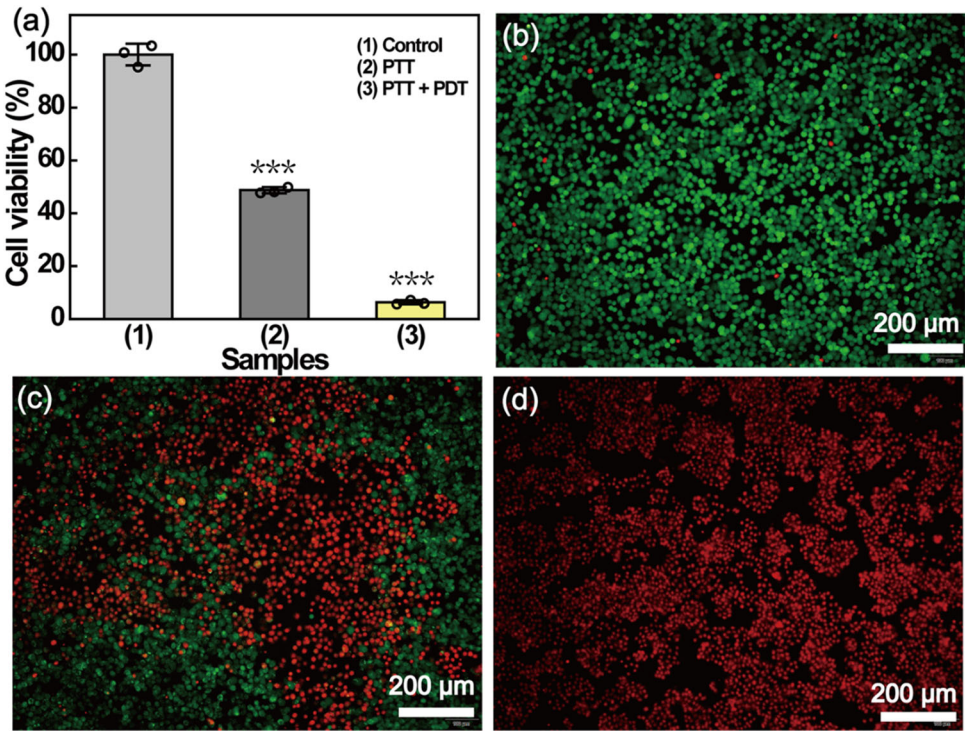

Figure 5 **a** The survival rate of HT29 cells after the PTT or the combined PTT/PDT; **b**–**d** phase-contrast pictures of HT29 cells after Dead/Live staining (**b**: control, **c**: PTT, and **d** PTT + PDT).

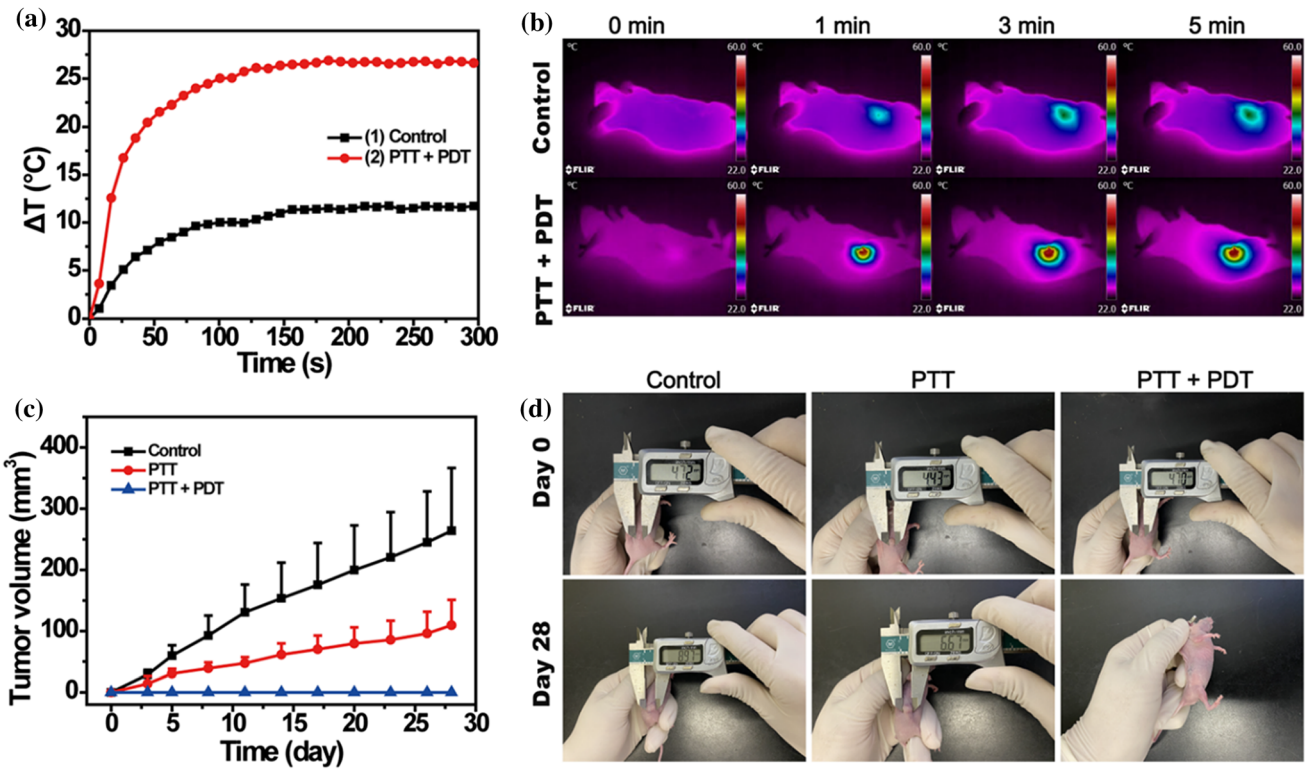

Figure 6 **a** The tumor temperature under NIR laser irradiation; **b** thermal imaging of mice after laser irradiation at different time points; **c** tumor volume of mice upon receiving different treatments; **d** pictures of mice at days 0 and 28 of the panel **c**.

recurrence in the CDM/IR808 + NIR group was almost suppressed, further indicating the high synergistic PDT/PTT treatment efficiency in vivo. In contrast, the tumors of the mice in the control group recurred and grew rapidly, with a new tumor with a size of 264.14 ± 102.21 mm^3 after 28 days of feeding. Histological analysis of H&E staining illustrated that the tumors in the test groups exhibited a scar-like structure containing numerous collagen bundles (Fig. 7a–c). The number of apoptotic cells in the combined therapy group was significantly higher than control (Fig. 7f–d). In TUNEL and Ki-67 assays, the results showed that the sections of the control group exhibited more tumor cell proliferation than the PTT and PTT + PDT groups, and the tumor cell proliferation content of the PTT + PDT group was the least obvious (Fig. 7g–i).

Conclusions

In summary, a multifunctional manganese-containing hydrogel (CDM/IR808) as a carrier was prepared for the loading of the photosensitizer, IR808. The synthesis of CMC-DA is based on the EDC/NHS coupling chemistry, during which the carboxyl group of the CMC-Na backbone and the amino group of DA underwent an amidation reaction. The $KMnO_4$ can not only be used as an oxidant to trigger the polymerization and gelation of CMC-DA but also transformed into MnO_2 and MnO to afford the T_2-weighted MRI. Under the single 808 nm laser irradiation, the CDM/IR808 hydrogel transformed the near-infrared light into heat energy and caused the hyperthermia killing of cancer cells. Moreover, the loaded IR808 converted the oxygen into cytotoxic ROS to further kill cancer cells. Therefore, the CDM hydrogel was used for the PDT and PTT combined prevention of postoperative tumor recurrence. With the proven hemo- and cyto-compatibility, the CDM and CDM/IR808 hydrogels in this research provide

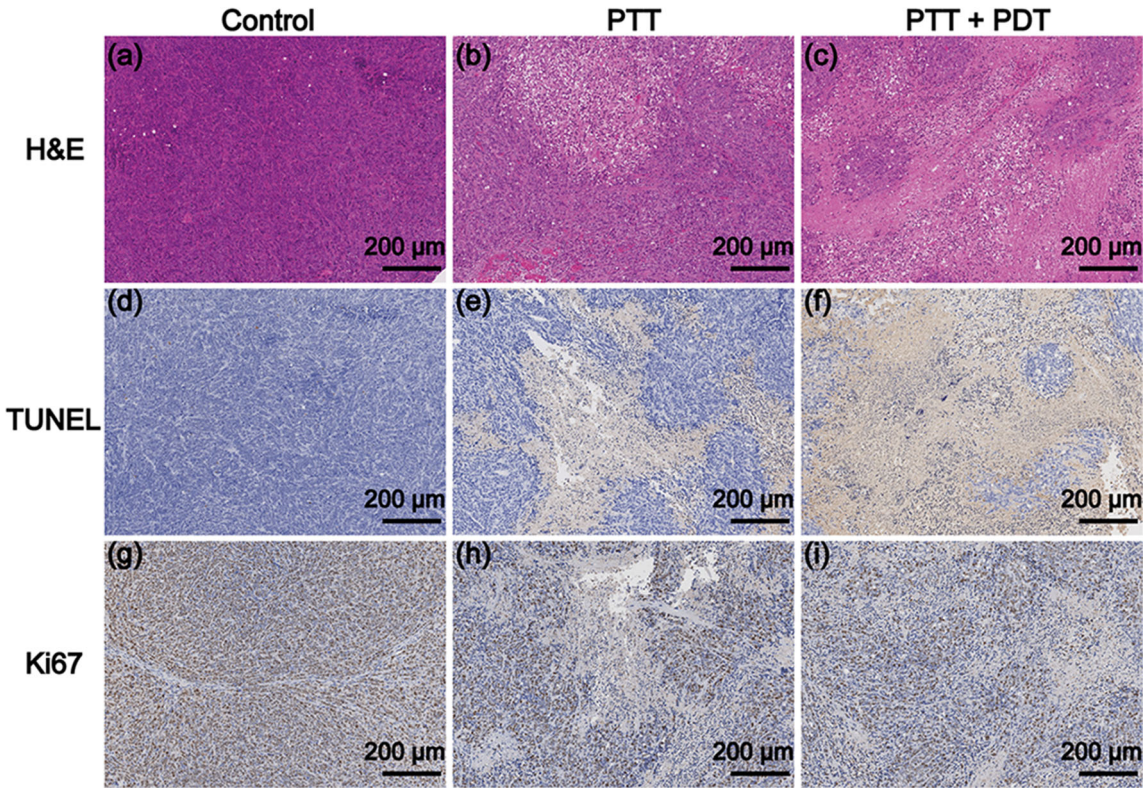

Figure 7 H&E sections of tumors after treatment of **a** PBS, **b** PTT, **c** PTT + PDT; TUNEL immunofluorescent images of tumors after treatment of **d** PBS, **e** PTT, **f** PTT + PDT; Ki67 immunohistochemical image of tumors after treatment of **g** PBS, **h** PTT, **i** PTT + PDT.

proofs for the rational design of multifunctional hydrogels.

Funding

This study was funded by Key cultivation projects of Gastroenterology, SHBY201904 (Yangbei Zhu).

Declaration

Conflict of interest The authors declare that they have no known competing financial interests or personal relationships that could have appeared to influence the work reported in this paper.

Supplementary Information: The online version contains supplementary material available at https://doi.org/10.1007/s10853-022-08046-2.

References

[1] Xie P, Zhang L, Shen H, Wu H, Zhao J, Wang S, Hu L (2022) Biodegradable $MoSe_2$-polyvinylpyrrolidone nanoparticles with multi-enzyme activity for ameliorating acute pancreatitis. J Nanobiotechnol 20(1):113

[2] Cheng Y, Zheng X, Zhang L, Zhao J, Hu L, Wang S (2023) Enhanced photothermal and chemotherapy of pancreatic tumors by degrading the extracellular matrix. Colloids Surf. B 221:113010

[3] Xie J, Fan T, Kim JH, Xu Y, Wang Y, Liang W, Qiao L, Wu Z, Liu Q, Hu W, Yin N, Yang L, Liu L, Kim JS, Zhang H (2020) Emetine-loaded black phosphorus hydrogel sensitizes tumor to photothermal therapy through inhibition of stress granule formation. Adv Funct Mater 30(43):2003891

[4] Zhou L, Wu Y, Meng X, Li S, Zhang J, Gong P, Zhang P, Jiang T, Deng G, Li W, Sun Z, Cai L (2018) Dye-anchored MnO nanoparticles targeting tumor and inducing enhanced phototherapy effect via mitochondria-mediated pathway. Small 14(36):1801008

[5] Liu P, Peng Y, Zhou Y, Shi X, Li Q, Ding J, Gao Y, Zhou W (2021) Rapamycin as a "One-Stone-Three-Birds" agent for cooperatively enhanced phototherapies against metastatic breast cancer. ACS Appl Mater Inter 13(22):25674–25684

[6] Guo L, Yan DD, Yang D, Li Y, Wang X, Zalewski O, Yan B, Lu W (2014) Combinatorial photothermal and immuno cancer therapy using chitosan-coated hollow copper sulfide nanoparticles. ACS Nano 8(6):5670–5681

[7] Hu J-J, Cheng Y-J, Zhang X-Z (2018) Recent advances in nanomaterials for enhanced photothermal therapy of tumors. Nanoscale 10(48):22657–22672

[8] Leitao MM, de Melo-Diogo D, Alves CG, Lima-Sousa R, Correia IJ (2020) Prototypic heptamethine cyanine incorporating nanomaterials for cancer phototheragnostic. Adv Healthc Mater 9(6):1901665

[9] Park YI, Kim HM, Kim JH, Moon KC, Yoo B, Lee KT, Lee N, Choi Y, Park W, Ling D, Na K, Moon WK, Choi SH, Park HS, Yoon S-Y, Suh YD, Lee SH, Hyeon T (2012) Theranostic probe based on lanthanide-doped nanoparticles for simultaneous in vivo dual-modal imaging and photodynamic therapy. Adv Mater 24(42):5755–5761

[10] Xu J, Han W, Yang P, Jia T, Dong S, Bi H, Gulzar A, Yang D, Gai S, He F, Lin J, Li C (2018) Tumor microenvironment-responsive mesoporous MnO_2-coated upconversion nanoplatform for self-enhanced tumor theranostics. Adv Funct Mater 28(36):1803804

[11] Escudero A, Carrillo-Carrion C, Castillejos MC, Romero-Ben E, Rosales-Barrios C, Khiar N (2021) Photodynamic therapy: photosensitizers and nanostructures. Mater Chem Front 5(10):3788–3812

[12] Cheng Y, Cheng H, Jiang C, Qiu X, Wang K, Huan W, Yuan A, Wu J, Hu Y (2015) Perfluorocarbon nanoparticles enhance reactive oxygen levels and tumour growth inhibition in photodynamic therapy. Nat Commun 6:8785

[13] Li X, Kwon N, Guo T, Liu Z, Yoon J (2018) Innovative strategies for hypoxic-tumor photodynamic therapy. Angew Chem Int Edit 57(36):11522–11531

[14] Yang J-C, Shang Y, Li Y-H, Cui Y, Yin X-B (2018) An "all-in-one" antitumor and anti-recurrence/metastasis nanomedicine with multi-drug co-loading and burst drug release for multi-modality therapy. Chem Sci 9(36):7210–7217

[15] Liu J, Zhao X, Nie W, Yang Y, Wu C, Liu W, Zhang K, Zhang Z, Shi J (2021) Tumor cell-activated "Sustainable ROS Generator" with homogeneous intratumoral distribution property for improved anti-tumor therapy. Theranostics 11(1):379–396

[16] Lan M, Zhao S, Liu W, Lee C-S, Zhang W, Wang P (2019) Photosensitizers for photodynamic therapy. Adv Healthc Mater 8(13):1900132

[17] Wang C, Wang X, Dong K, Luo J, Zhang Q, Cheng Y (2016) Injectable and responsively degradable hydrogel for personalized photothermal therapy. Biomaterials 104:129–137

[18] Wu L, Ishigaki Y, Zeng W, Harimoto T, Yin B, Chen Y, Liao S, Liu Y, Sun Y, Zhang X, Liu Y, Liang Y, Sun P, Suzuki T, Song G, Fan Q, Ye D (2021) Generation of hydroxyl radical-activatable ratiometric near-infrared bimodal probes for early monitoring of tumor response to therapy. Nat Commun 12(1):6145

[19] Hai J, Zeng X, Zhu Y, Wang B (2019) Anions reversibly responsive luminescent nanocellulose hydrogels for cancer spheroids culture and release. Biomaterials 194:161–170
[20] Chen Z, Wu H, Wang H, Zaldivar-Silva D, Aguero L, Liu Y, Zhang Z, Yin Y, Qiu B, Zhao J, Lu X, Wang S (2021) An injectable anti-microbial and adhesive hydrogel for the effective noncompressible visceral hemostasis and wound repair.Mater Sci Eng C 129:112422
[21] Wang T, Yi W, Zhang Y, Wu H, Fan H, Zhao J, Wang S (2023) Sodium alginate hydrogel containing platelet-rich plasma for wound healing. Colloids Surf. B 222:113096
[22] Du H, Liu W, Zhang M, Si C, Zhang X, Li B (2019) Cellulose nanocrystals and cellulose nanofibrils based hydrogels for biomedical applications. Carbohyd Polym 209:130–144
[23] Teixeira MA, Paiva MC, Amorim MTP, H.P. (2020) Felgueiras, Electrospun nanocomposites containing cellulose and its derivatives modified with specialized biomolecules for an enhanced wound healing. Nanomaterials 10(3):557
[24] Chiang C-W, Hsiao Y-C, Jheng P-R, Chen C-H, Manga YB, Lekha R, Chao K-M, Ho Y-C, Chuang E-Y (2021) Strontium ranelate-laden near-infrared photothermal-inspired methylcellulose hydrogel for arthritis treatment. Mater Sci Eng C 123:111980
[25] Samyn P (2021) Polydopamine and cellulose: two biomaterials with excellent compatibility and applicability. Polym Rev 61(4):814–865
[26] Xu Q, Chang M, Zhang Y, Wang E, Xing M, Gao L, Huan Z, Guo F, Chang J (2020) PDA/Cu bioactive hydrogel with "Hot Ions Effect" for inhibition of drug-resistant bacteria and enhancement of infectious skin wound healing. ACS Appl Mater Inter 12(28):31255–31269
[27] Poinard B, Neo SZY, Yeo ELL, Heng HPS, Neoh KG, Kah JCY (2018) Polydopamine nanoparticles enhance drug release for combined photodynamic and photothermal therapy. ACS Appl Mater Inter 10(25):21125–21136
[28] Zhang Y, Zhu C, Zhang Z, Zhao J, Yuan Y, Wang S (2021) Oxidation triggered formation of polydopamine-modified carboxymethyl cellulose hydrogel for anti-recurrence of tumor. Colloids Surf. B 207:112025
[29] Huang H, Feng W, Chen Y (2021) Two-dimensional biomaterials: material science, biological effect and biomedical engineering applications. Chem Soc Rev 50:11381–11485
[30] Zhong Y, Wang J, Yuan Z, Wang Y, Xi Z, Li L, Liu Z, Guo X (2019) A mussel-inspired carboxymethyl cellulose hydrogel with enhanced adhesiveness through enzymatic crosslinking. Colloids Surf. B 179:462–469
[31] Guo L, Liu W, Niu G, Zhang P, Zheng X, Jia Q, Zhang H, Ge J, Wang P (2017) Polymer nanoparticles with high photothermal conversion efficiency as robust photoacoustic and thermal theranostics. J Mater Chem B 5(15):2832–2839
[32] Yang X, Wang S, Zhang X, Ye C, Wang S, An X (2022) Development of PVA-based microsphere as a potential embolization agent. Mater Sci Eng C 135:112677
[33] Deng X, Huang B, Wang Q, Wu W, Coates P, Sefat F, Lu C, Zhang W, Zhang X (2021) A mussel-inspired antibacterial hydrogel with high cell affinity, toughness, self-healing, and recycling properties for wound healing. ACS Sustain Chem Eng 9(8):3070–3082
[34] Huang W, Cheng S, Wang X, Zhang Y, Chen L, Zhang L (2021) Noncompressible hemostasis and bone regeneration induced by an absorbable bioadhesive self-healing hydrogel. Adv Funct Mater 31(22):2009189
[35] Li K-C, Chu H-C, Lin Y, Tuan H-Y, Hu Y-C (2016) PEGylated copper nanowires as a novel photothermal therapy agent. ACS Appl Mater Inter 8(19):12082–12090
[36] Gao S, Zhou H, Cui S, Shen H (2018) Bottom-up synthesis of MoS_2 nanospheres for photothermal treatment of tumors. Photochem Photobiol Sci 17(10):1337–1345
[37] Yu B, Wang C (2020) Tunable synthesis of mesoporous prussian blue@calcium phosphate nanoparticles for synergic chemo-photothermal cancer therapy. ChemistrySelect 5(35):10841–10847
[38] Tang Z, Miao Y, Zhao J, Xiao H, Zhang M, Liu K, Zhang X, Huang L, Chen L, Wu H (2021) Mussel-inspired biocompatible polydopamine/carboxymethyl cellulose/polyacrylic acid adhesive hydrogels with UV-shielding capacity. Cellulose 28(3):1527–1540
[39] Cai X, Jia X, Gao W, Zhang K, Ma M, Wang S, Zheng Y, Shi J, Chen H (2015) A versatile nanotheranostic agent for efficient dual-mode imaging guided synergistic chemo-thermal tumor therapy. Adv Funct Mater 25(17):2520–2529
[40] Tsai Y-C, Vijayaraghavan P, Chiang W-H, Chen H-H, Liu T-I, Shen M-Y, Omoto A, Kamimura M, Soga K, Chiu H-C (2018) Targeted delivery of functionalized upconversion nanoparticles for externally triggered photothermal/photodynamic therapies of brain glioblastoma. Theranostics 8(5):1435